TIME-LAPSE MICROSCOPY AND CLASSIFICATION OF IN VITRO CELL MIGRATION USING HIDDEN MARKOV MODELING

K. Althoff, J. Degerman, C. Wählby, T. Thorlin, J. Faijerson, P.S. Eriksson, and T. Gustavsson

ABSTRACT

This paper describes a system for *in vitro* cell migration analysis. Adult neural stem/progenitor cells are studied using time-lapse microscopy and thereafter stained immunohistochemically to find and distinguish between undifferentiated glial progenitor cells and cells having differentiated into type-1 or type-2 astrocytes. The cells are automatically segmented and tracked throughout the time-lapse sequence. The evaluation showed that 88% of the cells were correctly segmented and tracked by the automatic system. Upon characterization of the cell migration by Hidden Markov Modeling, it was found that the motion of glial progenitor cells was random 2/3 of the time, while the type-2 astrocytes showed a directed movement 2/3 of the time. This finding indicates possibilities for cell-type specific identification and cell sorting of live cells based on specific movement patterns in individual cell populations, which will have valuable applications in neurobiological research.

1. INTRODUCTION

Cell migration analysis is of interest in many different biological applications, e.g. when studying leucocytes [1], fibroblasts [2], or unicellular microorganisms [3]. The overall aim of this project is to aid in the investigation of the mechanisms behind differentiation of neural stem/progenitor cells by creating a system for analyzing the motion of cells *in vitro*. Multipotent stem/progenitor cells derived from adult rat hippocampus, AHPs (Adult Hippocampal Progenitors), are capable of differentiating into neurons, astrocytes or oligodendrocytes, *in vitro*, as well as *in vivo*, after being transplanted into the adult brain [4]. They also possess several medically interesting features, such as the ability to survive and migrate, as well as become integrated into an injured brain without causing tumor formation.

The first step in our system is the image acquisition of developing neural stem/progenitor cells using time-lapse microscopy. Thereafter, the individual cells in each image are automatically segmented. Previous investigations,[5] led us to believe that seeded watershed segmentation combined with rule-based merging might be a suitable technique for identifying and segmenting individual cells. This choice of method was mainly motivated by the appearance of the cells at hand and the relatively low sampling rate. For solving the problem of cell tracking, we propose a combination of the nearest-neighbor and correlation matching techniques. Also, the tracking result should be used for improving the segmentation. The classification of the cells is based on preliminary observations [5] showing that a single cell may switch between different migration modes or states of migration in a random manner. Hidden Markov Modeling (HMM) is known to be a powerful statistical tool for describing non-stationary stochastic processes. There are reasons to believe that cell migration can be modelled as a random walk (Brownian motion) with sudden changes in step length or direction. Therefore, we have chosen a HMM for the migration analysis.

Karin Althoff, Johan Degerman, and Tomas Gustavsson are with the Department of Signals and System, Chalmers University of Technology, S-412 96 Gothenburg, Sweden. (email: johan.degerman@s2.chalmers.se)

Carolina Wählby, are with the Centre for Image Analysis, Uppsala University, S-752 37 Uppsala, Sweden.

Jonas Faijerson, Thorleif Thorlin, and Peter S. Eriksson are with the Arvid Carlsson Institute for Neuroscience at the Institute of Clinical Neuroscience, Sahlgrenska Academy, S-413 45 Gothenburg.

This project was partly funded by the Swedish Foundation for Strategic Research (SSF) under the VISIT program, No. A30-960626, the Swedish Research Council (VR), No. 621-2001-3531 and Swedish Scientific Council (Peter Eriksson, 12X-12535).

2. MICROSCOPE SETUP

A Leica DM IRB inverted light microscope with a 20X ordinary bright field objective and a 100W halogen lamp was used for imaging. Images are captured by a Microimager II CCD video camera from QImaging with 1.28 megapixels resolution, using a binning of size 2×2. The specimen is moved in the horizontal plane by a motorized microscope stage (Prior H107) to image the separate wells, and focus is set by a motorized focus drive, both controlled by a controller unit (Prior Proscan) that supports high-level text commands via a serial interface. The system does not have absolute position, however unipolar stepper motors assure that errors are not accumulating, and the repeatability is good enough for the present application. Auto-focusing is done by capturing a focus stack of 128 images with an interval of $0.5\mu m$ ($\sim$half the depth of field) and storing the image with the highest Brenner focus function score. Since no contrast enhancement technique is used, a certain level of de-focusing is needed to increase contrast, and meet the prerequisites for the segmentation. Hence the dual peak appearance of the focus curve.

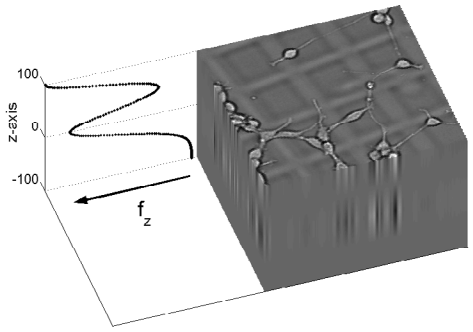

Fig. 1. An illustration of the image stack and the focus function f_z. The contrast of the image is maximized for a certain level of defocusing.

2.1. Horizontal motion correction

Since errors in the stage stepper motors do not accumulate the horizontal correction can be done by post-processing, as long as the error is small enough. Backlash and mechanical inertia is less evident in the stage than in the microscope focus control. The drifts in the x and y direction were random but differed in magnitude. For estimation of the translation for each pair of frames we compute the correlation $D_{t,t+1}$ in the Fourier domain, see Fig. 2(a).

$$D_{t,t+1} = FFT\{I(t)\} \cdot conj\,(FFT\{I(t{+}1\})) \qquad (1)$$

For two identical images, shifted x_d and y_d in the spatial domain, the phase of the correlation in the frequency domain will contain the translation in accordance with the Fourier shift theorem. Hence, the inverse transform of the phase of the correlation will have an energy distribution in which the center of gravity corresponds to the direction and magnitude of the translation.

$$d_{t,t+1} = IFFT\{e^{i\angle D}\} \qquad (2)$$

To sharpen the peak in Fig. 2(b), the central 32×32 part of $d_{t,t+1}$ was cropped, Fourier transformed, padded with zeros to 256×256, and finally inverse Fourier transformed. To obtain a well defined peak we use $d = |d|^{\alpha}$ with $\alpha = 10$. The drift of the stage is the cumulative sum over time of the center of gravity of $d_{t,t+1}(x, y)$.

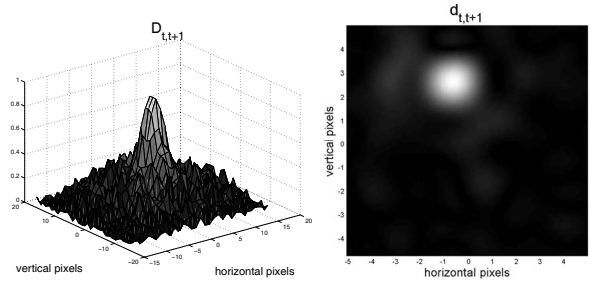

(a) (b)

Fig. 2. (a) The central part of $|D_{t,t+1}|$ in the fourier domain (b) $d_{t,t+1}$ in the spatial domain. In this example, the horizontal shift is -0.66 pixels and the vertical shift is 2.64 pixels.

The images used in this paper were 30 different image sequences acquired at two different occasions. Each image sequence contained 273 8-bit gray scale frames, each of size 634×504 pixels. One pixel corresponds to an area of $0.6 \times 0.6\ \mu m^2$ of the specimen. Images were acquired every 10 minutes for 45.5 hours. Thereafter the cells were immunostained for the A2B5 antigen and GFAP, in order to identify three different cell types: glial progenitor cells, type-1 astrocytes, and type-2 astrocytes.

3. SEGMENTATION

The image segmentation is based on seeded watershed segmentation. First, seeds representing objects (cells) and background are defined. The background is defined as a region with low local variance, while the cells, and their immediate surroundings, show greater variance. The variance at each pixel, is computed over a square neighborhood of size 9×9 of the gray level image (see Fig 3(b)) and the pixels below a manually set threshold level of $t_{bg} = 150$ were considered as background.

Object seeds were found using the h-maxima transform. The extended h-maxima transform filters out local maxima using a contrast criterion. All maxima with heights smaller than a threshold level h are suppressed. A low h will result in many seeds, often more than one seed per cell, while a high h will leave some cells without a seed. Due to a subsequent merging step (described below), we can accept extensive seeding and use a rather low h value (h=20). The choice of h turns out not to be a critical operation, since a range of values yield satisfactory results. All foreground seeds are uniquely labelled using connected component labelling.

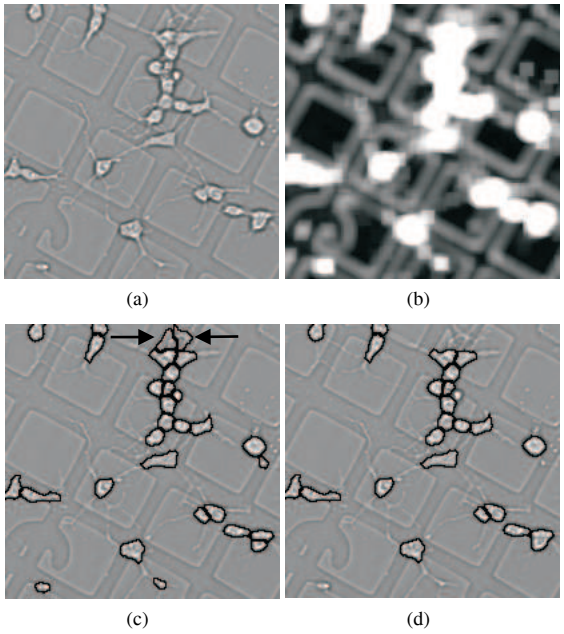

(a) (b) (c) (d)

Fig. 3. A (200×200 pixels) portion of the full field of view (634×504 pixels) showing the steps in the segmentation process. (a) The original image. (b) The variance map, used for definition of the background seed. (c) The result of seeded watershed segmentation; some objects that are not true cells are also detected. The arrows mark two false objects removed by subsequent merging. (d) The final segmentation result obtained by the described method.

Seeded watershed segmentation can be described by interpreting the intensity image as a landscape, where each isolated catchment basin will give rise to a watershed. In our case, we apply seeded watershed segmentation to the inverse of the original gray-scale image, and thus consider the dark edges of the cells as ridges, and the brighter cells and background as valleys. Each foreground and background seed will give rise to a watershed. The watershed segmentation is implemented using sorted pixel lists, and the resulting segmentation of Fig. 3(a) is shown in Fig. 3(c).

Extensive seeding results in partial over-segmentation. This over-segmentation is reduced by removing region boundaries crossing bright parts of the image, e.g., a boundary dividing a bright cell in two. We refer to this as merging regions with weak borders [6], and continue the merging until the average intensity along the border of all remaining objects is darker than a given threshold $t_m = 5$. This step will not only reduce over-segmentation, but also merge false objects, such as debris, with the background.

Despite the extensive seeding, some cells may be missed due to

weak diffraction of light. Cells may also be lost in the merging step. These cells are given a "second chance" of being found by a search in the variance map. Regions where no cell was found despite of high variance are further processed using morphological opening on a binary mask of the missed regions, detecting new cell-like regions. The final segmentation is shown in Fig. 3(d).

4. CELL TRACKING

In this section the different parts of the tracking system are described. The tracking is performed backwards, starting at frame 273, since the information about what kinds of cells the stem/progenitor cells have become is given by immunostaining subsequent to acquiring the last frame. One iteration in the algorithm can be described as solving the assignment problem, examine unassigned tracks, and examine unassigned objects and update results.

The asymmetric assignment problem, i.e. the problem of matching m objects with n tracks in an optimal way when $n \neq m$, can be formulated as:

$$\max \sum_{i=0}^{n} \sum_{j=0}^{m} a_{ij} x_{ij} \quad \forall (i,j) \in \Gamma \tag{3}$$

where a_{ij} is an assignment weight (i.e. the benefit of matching track i with object j), Γ is the set of pairs (i,j) that can be matched and x_{ij} is 1 if track i is assigned to object j and 0 otherwise.

Track i=0 and object j=0 are called the dummy track and the dummy object, respectively. The assignment is a one-to-one assignment, except for the dummy track and the dummy object which are allowed multiple assignments. Based on the results of Blackman & Popoli, (3) was solved using the modified auction algorithm. The assignment weights, a_{ij}, are calculated according to:

$$a_{ij} = \left(C_1 \frac{1}{\delta_{ij}} + C_2 \phi_{ij} + C_3 \frac{1}{\psi_{ij}} \right) \cdot w_i \tag{4}$$

where δ_{ij}, ϕ_{ij} and ψ_{ij} are explained below, and w_i is the weight for track i. Initially $w_i = 1$.

δ_{ij}, is a function depending estimating the distance between object j and the last known object in track i plus a small constant term to avoid the denominator becoming zero.

ϕ_{ij} is a the peak value of the normalized image correlation between the track and object images, using only pixels belonging to the segmented objects.

The last function, ψ_{ij}, is the difference in area of object j and the last known object in track i normalized by the area of object in track i, plus a small constant. The area contribution is limited by a maximum constant value C_4.

Constants C_1, C_2, C_3 and C_4 should be chosen so that two, not so similar, cells in consecutive frames with centroids closer than about half a typical cell radius ($r_{cell} \sim$ 7pixels) get a higher assignment weight than two cells further apart but very alike. In these investigations, suitable values for C_1, C_2, C_3 and C_4 were found to be 33, 5, 1 and 3 respectively. These values yield a maximum value of $C_2\phi_{ij} + C_3/\psi_{ij} = C_2 + C_4 = 8$, which means that δ_{ij} will always give the largest contribution to the assignment weight for distances between two cells of up to ~ 4 pixels ($\frac{33}{4} > 8$).

4.1. Unassigned tracks and objects

There are four reasons as to why a track might not get assigned to a real object (i.e. are assigned to the dummy object), they are: Mitosis (cell division) has occurred, cells disappear outside boundaries, cells disappear into clusters, or the segmentation was incorrect.

A division (or merge, since tracking is made backwards) of cell α at time t into two cells β_1 and β_2 at time $t+1$ is considered plausible if the following criteria are fulfilled: The total area of cells β_1 and β_2 is not 20% larger or 20% smaller than the area of cell α. The mean intensity of the interior of cell α is at least twice the mean intensity of the contour of cell α (since the spherical shape of the cell enhances the diffraction and hence also the contrast). Furthermore, cell α must be fairly circular i.e. the relationship between the major and minor axis of an ellipse with the same normalized second central moments as cell α should be at least 2/3.

If a cell is lost near the border or in a cluster, the the track weight w_i is gradually decreased and the the track is finally removed. A cell is considered to have disappeared into a cell cluster if the track is not near an image border, and if no segmentation error or merging of cells could be detected.

In the first three cases, the track should be terminated. In the clustering case a new segmentation is performed, using border tracing with dynamic programming is performed, see [7] for details. If the result satisfy a number of requirements regarding the object size and contour intensity, the cell is regarded as valid and assigned to the track, otherwise the cell is assumed to have joined a cluster.

Furthermore, there are three possible cases of unassigned objects appearing in an image: cells appearing from outside the image boundaries, cells previously hidden in a cell cluster, or falsely detected cells. If the center of an unassigned cell is closer than 11 pixels from any of the image borders, it is assumed to have appeared from outside the image and a new track is started. A new track is also started for objects emerging from clusters if they are fulfilling the criteria for valid cells. If an unassigned object does not satisfy the criteria and is further than 11 pixels away from the border, it is likely that it is not a cell and a new track is started but given a low track weight. However, if no cell can be associated with the track in the next frame, it is deleted from both frames.

5. MIGRATION MODELING

Preliminary experiments suggest that the cells switch between Brownian motion and directed movement [5]. To model the movement, we applied a discrete Hidden Markov Model with two states. The model consists of the probability distributions of the states and the probability of switching between these states at each time instance. The method developed by Baum et. al. assures convergence to a local maximum of the maximum likelihood estimate of the model. The parameters used as input for the model were the speed of the cells, $s_i(t)$, and the angular change in movement, $\theta_i(t)$, calculated for every position throughout the sequence, see Fig. 4, and then discretized into 10 bins. Before $s_i(t)$ and $\theta_i(t)$ was calculated the cell positions were filtered using an averaging filter. The next step was to

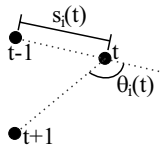

Fig. 4. Angle and speed of cell track i at time t. The black dots represents the average filtered location of the cell at time t-1, t and t+1. Note that since the time interval between two consecutive frames is constant, the speed equals the distance.

determine the state that each cell occupies for all times throughout the sequence. This is called the decoding problem, and the Viterbi algorithm, was used to find the most probable path, given the HMM.

6. RESULTS AND DISCUSSION

The total number of cells that were correctly segmented and tracked over time divided by the total number of tracked cells over time was 87.7%. The error rates were distributed as follows: over-segmentation 1.7%, under-segmentation 3.5%, partially detected objects 0.4%, missed cells 5.3%, and tracking errors 1.4%. The difference in manual corrections made by two different users correcting the same sequence, i.e. inter-observer variability, was estimated to 2.5%. This can be used as a measure of the variance of the error rate of the corrected sequences.

Of the 30 sequences acquired, only 17 contained cells that responded to the immuno staining. A total of 133 glial progenitor cells were found, and they were present in 157 image frames on average. The corresponding numbers for the type-1 and type-2 astrocytes were 20 cells and 83 image frames, and 28 cells and 117 image frames, respectively. The cells classified in the fluorescent images were manually identified in the last image of their corresponding image sequence.

For all 180 stained cells, $s_i(t)$ and $\theta_i(t)$ (see Fig. 4) were calculated and used as input for the HMM model. We found, using several different initial assumptions of the state probability distributions, that two distinct states are present. The two variables are assumed to be independent. The resulting probability distributions of the two states are shown i Fig. 5. The probability distributions

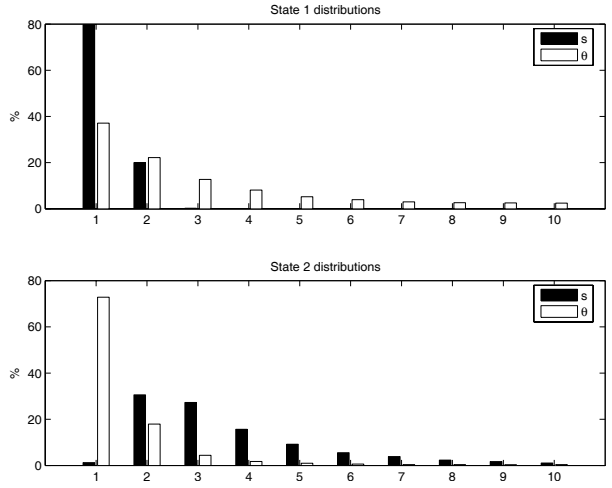

Fig. 5. Distribution of speed (dark columns) and angle difference (white columns) for state 1 and state 2. The speed interval is 0-9 pixels/frame and the angle interval is 0-180°.

shown in Fig. 5 suggest that state 1 represents a random motion with comparatively large changes in direction of motion. State 2 represents cells that exhibit a directed movement; their speed is higher while the direction of the motion changes less.

Using the Viterbi algorithm, the state of each cell at all times throughout the sequence was determined. When all the tracks of the stained cells had been decoded, the mean value of time spent in each state for the three different cell types was calculated. The result is shown in Fig. 6. From a biological viewpoint the most interesting

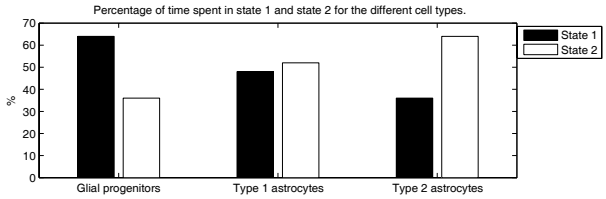

Fig. 6. Percentage of time spent in state 1 and 2 for the three different cell types.

finding is the distinct difference in motion patterns between the glial progenitors and type-2 astrocytes. Fig. 6 shows that the glial progenitor cells spend 2/3 of the time in state 1, moving more or less randomly, while type-2 astrocyte cells spend 2/3 of the time in state 2 exhibiting a more directed movement.

No conclusions can be drawn from the difference in result between the type-1 and type-2 astrocytes, as the number of type-1 astrocytes were small and they were present in fewer frames on average. We conclude that migration of glial progenitors is random almost twice as often as for cells that became type-2 astrocytes, which are more directional in their movement. The biological underpinnings of this phenomenon is not known, but one explanation could be that immature cells are more sensitive to secreted factors in the microenvironment and thus respond to conflicting chemotactic signals which cause the random behavior. Future work will hopefully provide us with more data, especially for the two types of astrocytes, to confirm these findings.

7. REFERENCES

[1] D.P. Mukherjee, N. Ray, and S.T. Acton, "Level set analysis for leukocyte detection and tracking," *IEEE Transactions on Image Processing*, vol. 13, no. 4, pp. 562–572, 2004.

[2] F. Leymarie and M.D. Levine, "Tracking deformable objects in the plane using an active contour model," *IEEE Transactions on Pattern Analysis and Machine Intelligence*, vol. 15, no. 6, pp. 617–634, 1993.

[3] C. Zimmer, E. Labruyere, V. Meas-Yedid, N. Guillen, and J.-C. Olivo-Marin, "Segmentation and tracking of migrating cells in videomicroscopy with parametric active contours: a tool for cell-based drug testing," *IEEE Transactions on Medical Imaging*, vol. 21, no. 10, pp. 1212–1221, 2002.

[4] T.D. Palmer, J. Takahashi, and F.H. Gage, "The adult rat hippocampus contains primordial neural stem cells," *Molecular and Cellular Neurosciences*, vol. 8, no. 6, pp. 389–404, 1997.

[5] T. Gustavsson, K. Althoff, J. Degerman, T. Olsson, A.-C. Thoreson, T. Thorlin, and P Eriksson, "Time-lapse microscopy and image processing for stem cell research modeling cell migration," in *Medical Imaging 2003: Image Processing*, 2003, vol. 5032, pp. 1–15.

[6] C. Wählby, I.-M Sintorn, F. Erlandsson, G. Borgefors, and E. Bengtsson, "Combining intensity, edge, and shape information for 2D and 3D segmentation of cell nuclei in tissue sections," *Journal of Microscopy*, vol. 215, no. 1, pp. 67–76, 2004.

[7] K. Althoff, J. Degerman, and T. Gustavsson, "Combined segmetnation and tracking of neural stem-cells," in *Proceedings of the 14th Scandinavian Conference on Image Analysis*, 2005.